

High- T_c Superconductivity near the Anion Height Instability in Fe-based Superconductors: Analysis of $\text{LaFeAsO}_{1-x}\text{H}_x$

Seiichiro ONARI¹, Youichi YAMAKAWA², and Hiroshi KONTANI²

¹ *Department of Applied Physics, Nagoya University, Furo-cho, Nagoya 464-8603, Japan.*

² *Department of Physics, Nagoya University, Furo-cho, Nagoya 464-8602, Japan.*

(Dated: September 13, 2018)

The isostructural transition in the tetragonal phase, with sizable change in the anion-height, is realized in heavily H-doped LaFeAsO and (La,P) co-doped CaFe_2As_2 . In these compounds, the superconductivity with higher- T_c (40 ~ 50K) is realized near the isostructural transition. To find the origin of the anion-height instability and the role in realizing the higher- T_c state, we develop the orbital-spin fluctuation theory by including the vertex correction. We analyze $\text{LaFeAsO}_{1-x}\text{H}_x$, and find that the non-nematic orbital fluctuations, which induce the anion-height instability, are automatically obtained at $x \sim 0.5$, in addition to the conventional nematic orbital fluctuations at $x \sim 0$. The non-nematic orbital order triggers the isostructural transition, and its fluctuation would be a key ingredient to realize higher- T_c superconductivity of order 50K.

PACS numbers: 74.70.Xa, 74.20.-z, 74.20.Rp

The normal-state phase diagram of Fe-based superconductors is important to reveal the essential electronic states and the mechanism of superconductivity. In many compounds, the structure transition from tetragonal (C_4) to orthorhombic (C_2) is realized at T_S , and the antiferromagnetic (AFM) order appears at T_N below T_S . The superconductivity is realized near the structural quantum critical point (QCP) at $T_S = 0$ and/or the magnetic QCP at $T_N = 0$. For example, the optimum T_c in $\text{FeSe}_x\text{Te}_{1-x}$ is realized near the structural QCP at $x \approx 0.6$ [1], whereas AFM order is absent for $x > 0.5$.

To explain the C_2 structure transition, both the spin-nematic [2] and orbital-nematic [3–7] mechanisms had been proposed. In the latter scenario, orbital-nematic order is induced by spin fluctuations, due to strong orbital-spin mode-coupling described by the vertex correction (VC) [6]. Both mechanisms can explain the shear modulus C_{66} softening [8, 9]. The orbital mechanism would be consistent with the large d -level splitting $E_{yz} - E_{xz} \sim 500\text{K}$ in the C_2 phase [10, 11], and with the large orbital susceptibility given by Raman spectroscopy [12, 13]. The nematic order is observed by the magnetic torque measurements [14]. Since the superconductivity is realized next to the orbital and spin ordered phases, both fluctuations would be essential for the pairing mechanism.

However, this is not the whole story of Fe-pnictides: The unique phase diagram of $\text{LaFeAsO}_{1-x}\text{H}_x$ with double-dome superconducting phase [15, 16] attracts great attention. The second superconducting dome ($x \geq 0.2$) is next to the “ C_4 isostructural phase transition” with sizable change in the c -axis length (or anion-height) for $0.45 < x < 0.5$ [17, 18]. (The c -axis length is unchanged in the C_2 structure transition at $x \sim 0$.) Similarly, high- T_c ($\sim 50\text{K}$) superconductivity is realized near the “collapsed C_4 phase” in rare-earth doped CaFe_2As_2 [19, 20]. In (La,P) co-doped CaFe_2As_2 , higher- T_c state is realized near the anion-height instability,

whereas it avoids the AFM phase as clearly shown in Ref. [19, 20]. These experiments strongly indicate that the anion-height instability is a key ingredient for higher- T_c superconductivity of order 50K. Authors in Ref. [21] discussed that the C_4 phase in $(\text{Ba},\text{Na})\text{Fe}_2\text{As}_2$ originates from the C_4 magnetic order. However, stripe magnetic order ($=C_2$ symmetry) is realized in $\text{LaFeAsO}_{1-x}\text{H}_x$ at $x \sim 0.5$ [17], which indicates small spin-lattice coupling.

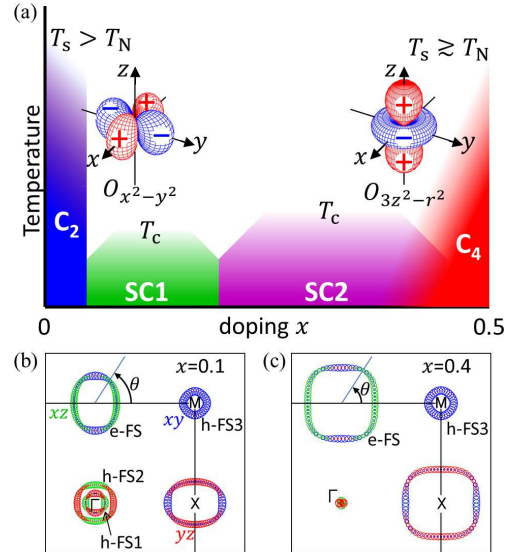


FIG. 1: (color online) (a) Schematic phase diagram of $\text{LaFeAsO}_{1-x}\text{H}_x$. We predict that non-nematic $O_{3z^2-r^2}$ (nematic $O_{x^2-y^2}$) charge quadrupole order emerges in the C_4 (C_2) phase. (b)(c) FSs at $x = 0.1$ and $x = 0.4$ [22]. e-FS is the electron-pocket, and h-FS3 (h-FS1,2) is the hole-pocket composed of d_{xy} (d_{xz} , d_{yz}) orbital.

In this paper, we discuss the origin of the anion-height instability and its role of higher- T_c superconductivity. For this purpose, we study $\text{LaFeAsO}_{1-x}\text{H}_x$ ($x = 0 \sim 0.5$) by calculating both the VC and the self-

energy Σ self-consistently. By this “self-consistent VC+ Σ (SC-VC $_{\Sigma}$) method”, we obtain the non-nematic orbital order $O_{3z^2-r^2}$ at $x \sim 0.5$. This order parameter couples to the anion-height change and triggers the C_4 isostructural transition, which cannot be explained by the spin-fluctuation theories without the VC [22–24]. We also find that orbital-fluctuation-mediated s -wave state is stabilized by including the VC for the gap equation, which is dropped in conventional Migdal-Eliashberg theory. The present study reveals that multiple kinds of orbital fluctuations play significant roles in Fe-based superconductors.

Figure 1 (a) shows the phase diagram of LaFeAsO $_{1-x}$ H $_x$: We propose that the charge quadrupole order $O_{3z^2-r^2} \equiv \frac{1}{2}(n_{xz} + n_{yz}) - n_{xy}$ ($O_{x^2-y^2} \equiv n_{xz} - n_{yz}$) appears at $x \sim 0.5$ ($x \sim 0$). The softening of the longitudinal modulus along the c -axis, C_{33} , observed in under- and over-doped Ba(Fe $_{1-x}$ Co $_x$) $_2$ As $_2$ [25] indicates that $O_{3z^2-r^2}$ quadrupole fluctuations exist in various Fe-based compounds.

The tight-binding model of LaFeAsO $_{1-x}$ H $_x$ for $0 \leq x \leq 0.5$ had been introduced by the present authors in Ref. [15]. The Fermi surfaces (FSs) for $x = 0.1$ and 0.4 are shown in Fig. 1 (b) and (c), respectively. The intra-orbital nesting and inter-orbital one are the driving forces of the magnetic and orbital fluctuations, respectively. We analyze the multiorbital Hubbard model with intra (inter) orbital interaction U (U') and the exchange interaction J under the constraint $U = U' + 2J$, assuming uniform states. Electronic phase separation due to the imperfect nesting is discussed in Ref. [26].

Here, we denote $d_{3z^2-r^2}$, d_{xz} , d_{yz} , d_{xy} , $d_{x^2-y^2}$ orbitals as 1, 2, 3, 4, 5. The FSs are mainly composed of 2,3,4 orbitals. The charge (spin) susceptibility $\hat{\chi}^{c(s)}(q)$ is given in the $5^2 \times 5^2$ matrix form in the orbital basis as follows:

$$\hat{\chi}^{c(s)}(q) = \hat{\Phi}^{c(s)}(q)(1 - \hat{\Gamma}^{c(s)}\hat{\Phi}^{c(s)}(q))^{-1} \quad (1)$$

where $q = (\mathbf{q}, \omega_l)$ and $\hat{\Phi}^{c(s)}(q) = \hat{\chi}^{(0)}(q) + \hat{X}^{c(s)}(q)$: $\hat{\chi}^{(0)}(q)$ is the bubble susceptibility with self-energy correction, and $\hat{X}^{c(s)}(q)$ is the VC for charge (spin) channel. $\hat{\Gamma}^{c(s)}$ is the matrix form of the bare Coulomb interaction for the charge (spin) sector [27]. In the original SC-VC $_{\Sigma}$ method, the VC is given by the Maki-Thompson (MT) and Aslamazov-Larkin (AL) terms, which are the first and second order terms with respect to $\hat{\chi}^{c,s}$, respectively. Since $\hat{X}^c \gg \hat{X}^s$ near the QCP, we put $\hat{X}^s(q) = 0$, and calculate only the AL term for $\hat{X}^c(q)$ self-consistently. Its justification is verified in Refs. [6, 28], and also confirmed by the recent renormalization group study [29].

The charge (spin) Stoner factor $\alpha_{c(s)}$ is given by the maximum eigenvalue of $\hat{\Gamma}^{c(s)}\hat{\Phi}^{c(s)}(q)$ in eq. (1), and $\alpha_{c(s)} = 1$ corresponds to the orbital (spin) order. Although the relation $\alpha_s \gg \alpha_c$ is satisfied within the RPA for $J > 0$, the opposite relation can be realized if the VC is taken into account beyond the RPA. Here, we intro-

duce the quadrupole susceptibilities:

$$\chi_{\gamma}^Q(\mathbf{q}, \omega_l) = \sum_{l,l',m,m'} O_{\gamma}^{l,l'} \chi_{l,l';m,m'}^c(\mathbf{q}, \omega_l) O_{\gamma}^{m',m}, \quad (2)$$

where $\gamma = x^2 - y^2$, $3z^2 - r^2$, xz , yz , xy represents the quadrupole [30]. Then, $\chi_{x^2-y^2}^Q(q) \approx \chi_{2,2;2,2}^c(q) + \chi_{3,3;3,3}^c(q) - 2\chi_{2,2;3,3}^c(q)$, and $\chi_{3z^2-r^2}^Q(q) \approx \chi_{4,4;4,4}^c(q) - \sum_{l=2,3} \chi_{l,l;4,4}^c(q) + \sum_{l,m=2,3} \chi_{l,l;m,m}^c(q)/4$.

Now, we study the tight-binding Hubbard models of LaFeAsO $_{1-x}$ H $_x$ based on the SC-VC $_{\Sigma}$ method, in which both the VC and the one-loop self-energy $\hat{\Sigma}$ are calculated self-consistently. By this method, the mass-enhancement factor for l -orbital is given as $1/z_l = 1 - \text{Re}d\Sigma_l(k, \omega)/d\omega|_{\omega=0}$, and we obtain $1/z_l = 3 \sim 5$ for $l = 2 \sim 4$ and $1/z_4 > 1/z_{2,3}$ in LaFeAsO $_{1-x}$ H $_x$. The expressions of the VC and $\hat{\Sigma}$ are explained in Refs. [31] in detail. Hereafter, we fix the parameters $J/U = 0.14$ and $T = 0.05\text{eV}$, and the unit of energy is eV.

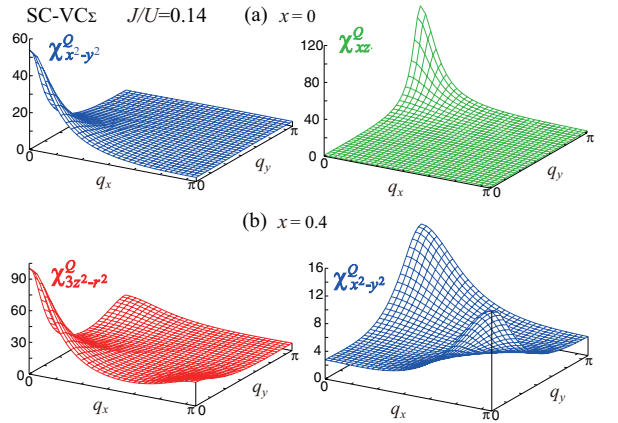


FIG. 2: (color online) $\chi_{\gamma}^Q(\mathbf{q})$ at zero frequency obtained by the SC-VC $_{\Sigma}$ method: (a) $\gamma = x^2 - y^2$ and $\gamma = xz$ for $x = 0$ ($U = 2.06$), and (b) $\gamma = 3z^2 - r^2$ and $\gamma = x^2 - y^2$ for $x = 0.4$ ($U = 1.65$). Note that $\chi_{xz}^Q(q_x, q_y) = \chi_{yz}^Q(q_y, q_x)$. Similar results are obtained by the SC-VC method [32].

Figure 2 shows the largest two static quadrupole susceptibilities $\chi_{\gamma}^Q(\mathbf{q})$ for (a) $x = 0$ and (b) $x = 0.4$, respectively. For each x , the relations $\alpha_c = 0.97$ and $a_c > \alpha_s \sim 0.9$ are satisfied, consistently with the relation $T_S > T_N$. At $x = 0$ in (a), we obtain the strong developments of $\chi_{x^2-y^2}^Q(\mathbf{0})$ and $\chi_{xz}^Q(\mathbf{Q})$, similarly to the previous SC-VC analysis [6]. The divergence of $\chi_{x^2-y^2}^Q(\mathbf{0})$ causes the C_2 structure transition. In addition, large antiferro-orbital fluctuations are induced by the cooperation of the VC and the good inter-orbital nesting between e-FS and h-FSs [6]. The shear modulus $C_{66} \propto 1 - g_{x^2-y^2} \chi_{x^2-y^2}^Q(\mathbf{0})$ reaches zero even if $\chi_{x^2-y^2}^Q(\mathbf{0})$ in the SC-VC $_{\Sigma}$ method is finite, where $g_{x^2-y^2} (\ll 1)$ is the quadrupole interaction due to the acoustic phonon [33].

At $x = 0.4$ in Fig. 2 (b), in contrast, we obtain the large peak of $\chi_{3z^2-r^2}^Q(\mathbf{0})$ due to the VC. Since its diver-

gence induces the change in the ratio n_{xy}/n_{xz} while keeping $n_{xz} = n_{yz}$, the obtained large $\chi_{3z^2-r^2}^Q(\mathbf{0})$ gives the non-nematic (C_4) orbital fluctuations and anion-height instability. In addition, large antiferro-orbital fluctuations $\chi_{x^2-y^2}^Q(\mathbf{Q})$ are also induced by the VC. It is noteworthy that a strong interorbital charge transfer from in-plane to out-of-plane orbitals is observed in Co-doped BaFe_2As_2 [34].

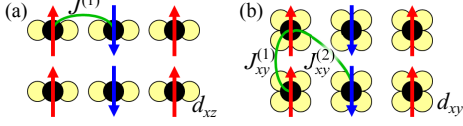


FIG. 3: (color online) (a) Localized (d_{xz}, d_{yz})-orbital model with KK coupling. (b) Localized d_{xy} -orbital model with Heisenberg coupling. Here, the occupied orbitals are shown.

Here, we try to understand the orbital-spin mode-coupling due to AL term in terms of the localized picture $U \gg W_{\text{band}}$: First, we introduce the Kugel-Khomskii (KK) type orbital-dependent exchange interaction [35] with the nearest neighbor d_{xz}, d_{yz} -orbitals, $H' \sim J^{(1)} \sum_{\langle i,j \rangle} (\mathbf{s}_i \cdot \mathbf{s}_j) (n_{xz}^i n_{xz}^j \delta_{i-j, (\pm 1, 0)} + n_{yz}^i n_{yz}^j \delta_{i-j, (0, \pm 1)})$, as shown in Fig. 3 (a). Note that $J^{(1)} \sim 2t^2/U$. Due to this orbital-spin coupling term, if the AFM order with $\mathbf{Q} = (\pi, 0)$ is realized, the electrons at each site will occupy the d_{xz} -orbital, as shown in Fig. 3 (a). That is, the AFM order or fluctuations induces the C_2 orbital order ($n_{xz} \neq n_{yz}$) or fluctuations, and vice versa. Next, we consider the single d_{xy} -orbital model with the nearest and next-nearest-neighbor exchange interactions: $H'' \sim J_{xy}^{(1)} \sum_{\langle i,j \rangle} (\mathbf{s}_i \cdot \mathbf{s}_j) (n_{xy}^i n_{xy}^j) + J_{xy}^{(2)} \sum_{\langle\langle i,j \rangle\rangle} (\mathbf{s}_i \cdot \mathbf{s}_j) (n_{xy}^i n_{xy}^j)$. When $J_{xy}^{(2)} > \frac{1}{2} J_{xy}^{(1)}$, the $\mathbf{Q} = (\pi, 0)$ AFM state in Fig. 3 (b) appears due to “order-by-disorder” mechanism [36].

Now, we consider the three-orbital model $H' + H''$: When $J_{xy}^{(2)} \gg J^{(1)}$, the ferro-orbital polarization $n_{xy} \gg n_{xz} = n_{yz}$ with AFM order shown in Fig. 3 (b) would be realized to gain the exchange energy. In this case, the AFM order or fluctuations induces non-nematic C_4 orbital order or fluctuations, and vice versa. This case corresponds to $x \sim 0.5$ with strong d_{xy} -orbital spin fluctuations. Thus, the KK-type spin-orbital coupling is understandable in term of the weak-coupling approach by including the AL term. The strong coupling approaches are useful to understand the ordered phases [37].

We also discuss why the VC induces the C_4 (C_2) order at $x = 0.5$ ($x = 0$) analytically: When spin fluctuations develop mainly in the l -orbital, the charge AL-term $X_{l,l,l,l}^c(\mathbf{0}) \sim T \sum_{\mathbf{k}} \{\chi_{l,l,l,l}^s(\mathbf{k})\}^2$ becomes large [6, 28]. Now, we analyze $\chi_{\gamma}^Q(\mathbf{0})$ by inputting only three irreducible susceptibilities $\Phi_l^c \equiv \chi_{l,l,l,l}^{(0)}(\mathbf{0}) + X_{l,l,l,l}^c(\mathbf{0})$ ($l = 2 \sim 4$) into eq. (1). For $J = 0$, for simplicity,

we obtain [28, 32]

$$\chi_{x^2-y^2}^Q(\mathbf{0}) = 2\Phi_2^c(1 - U\Phi_2^c)^{-1}, \quad (3)$$

$$\chi_{3z^2-r^2}^Q(\mathbf{0}) = b(1 - aU\Phi_4^c)^{-1}, \quad (4)$$

where $a \equiv (5U\Phi_2^c - 1)/(3U\Phi_2^c + 1)$ and $b \sim (5U\Phi_4^c + 1)^2/16U^2\Phi_4^c$ near the QCP. In the case of $\Phi_2^c = \Phi_3^c > a\Phi_4^c$, then $\chi_{x^2-y^2}^Q(\mathbf{0})$ is the most divergent. In the opposite case, $\chi_{3z^2-r^2}^Q(\mathbf{0})$ is the most divergent if a is positive. At $x \sim 0.4$, h-FS1 and h-FS2 almost disappear as shown in Fig. 1 (c), so d_{xy} -orbital spin fluctuations becomes dominant [22]. For this reason, at $x \sim 0.4$, the $O_{3z^2-r^2}$ order and anion-height instability are driven by Φ_4^c due to strong d_{xy} -orbital spin fluctuations.

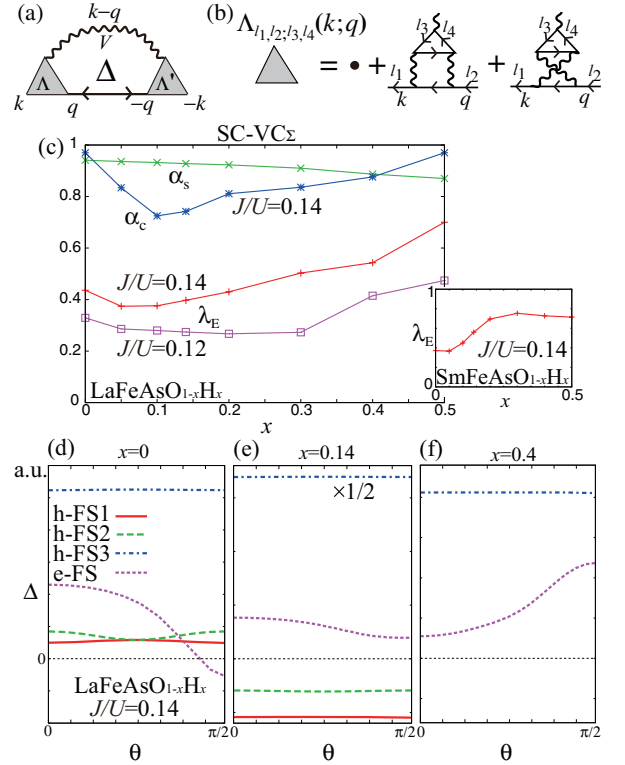


FIG. 4: (color online) (a) Gap equation with Δ -VC and (b) AL-type diagram for Λ . (c) $\alpha_{c,s}$ and λ_E as functions of x in $\text{LaFeAsO}_{1-x}\text{H}_x$ for $J/U = 0.14$. λ_E for $J/U = 0.12$ is also shown. (Inset: λ_E in $\text{SmFeAsO}_{1-x}\text{H}_x$.) The gap functions on the FSs at (d) $x = 0$, (e) $x = 0.14$ and (f) $x = 0.4$ for $J/U = 0.14$. θ is the azimuthal angle in Fig. 1 (b) and (c).

Now, we study the superconductivity due to orbital and spin fluctuations, based on the SC-VC_Σ method. In almost all previous studies, the VC for the gap equation (Δ -VC) had been dropped. In strongly correlated systems, however, Δ -VC could be quantitatively important since the Migdal’s theorem is not valid any more. Since the AL-type VC for $\chi_{\gamma}^Q(q)$ is very large, Δ -VC due to AL-type diagram should be significant. Here, we solve the following gap equation in the orbital-basis by taking

the Δ -VC into account:

$$\lambda_E \Delta_{l,l'}(k) = -T \sum_{q, m_i} V_{l, m_1; m_4, l'}(k, q) G_{m_1, m_2}(q) \times \Delta_{m_2, m_3}(q) G_{m_4, m_3}(-q) \quad (5)$$

where λ_E is the eigenvalue, $\Delta_{l,l'}(k)$ is the gap function, and $G_{l,l'}(q)$ is the Green function with self-energy. The pairing interaction $V_{l, m_1; m_4, l'}(k, q)$ is given as

$$\hat{V}(k, q) = \frac{3}{2} \hat{\Lambda}^s(k, q) \hat{\Gamma}^s \hat{\chi}^s(k - q) \hat{\Gamma}^s \hat{\Lambda}^s(-k, -q) - \frac{1}{2} \hat{\Lambda}^c(k, q) \hat{\Gamma}^c \hat{\chi}^c(k - q) \hat{\Gamma}^c \hat{\Lambda}^c(-k, -q) + V^{(1)}(6)$$

where $\hat{\Lambda}^{c(s)}(k, q)$ is the vertex for the charge (spin) channel shown in Fig. 4 (a), $\Lambda_{l, l'; m, m'}^{c(s)}(k, q) = \Lambda_{m', m; l', l}^{c(s)}(k, q)$, and $V^{(1)} = \frac{1}{2}(\hat{\Gamma}^s - \hat{\Gamma}^c) \sim U$. To make consistency with the SC-VC $_{\Sigma}$ method, we calculate the AL-type contribution to $\hat{\Lambda}^c(k, q)$ given in Fig. 4 (b), whereas we put $\hat{\Lambda}^s(k, q) = \hat{\Lambda}$.

To study the superconducting state for $x = 0 \sim 0.5$, we introduce $\bar{U}(x)$ by the linear interpolation between $U_c = 2.06$ at $x = 0$ and $U_c = 1.55$ at $x = 0.5$, as done in Ref. [22]. The obtained $\bar{U}(x)$ decreases with x , which will be given by the change in the Kanamori screening, which is dropped in the present one-loop Σ . In fact, the density of states at the Fermi level, $N(0)$, increases by 30%, by changing x from 0 to 0.5. In contrast, $\bar{U}(x)$ is a strong increasing function in the rigid band approximation [22]. Figure 4 (c) shows the obtained x -dependence of the $\alpha_{c,s}$ and λ_E for $J/U = 0.14$ by using $U = \bar{U}(x)$. The large α_c at $x = 0$ and that at $x = 0.5$ explain the experimental C_2 and C_4 structure transitions of $\text{LaFeAsO}_{1-x}\text{H}_x$. The eigenvalue λ_E approximately follows α_c and shows two peaks near the C_2 and C_4 structure transition points, due to the strong orbital fluctuations. Since T_c is suppressed by the structure transition, the obtained x -dependence of λ_E would be consistent with the double-dome T_c . In contrast, single-dome T_c is obtained in the FLEX approximation in the present model [32].

Figure 4 (d)-(f) show the gap functions multiplied by z_l in the band-basis for $x = 0, 0.14$ and 0.4 , respectively. At $x \sim 0$ and 0.4 , approximate s_{++} -wave states are obtained as shown in (d) and (f), due to the strong orbital fluctuations. At $x \sim 0.4$, the gap structure is fully-gapped, whereas the gap on the e-FS is nodal at $x \sim 0$ due to the competition (cooperation) of orbital and spin fluctuations [38]. These s_{++} -type gap structures are realized by taking the Δ -VC into account beyond the Migdal's theorem, since the attractive interaction due to $\hat{\chi}^c$ in eq. (6) is multiplied by $|\hat{\Lambda}^c(k, q)|^2 \gg 1$ [6, 31]. (The Δ -VC can overcome the factor 3 for the spin channel in eq. (6) that favors the s_{\pm} -state.) The s_{++} state is realized against the strong Coulomb repulsion due to the retardation effect, since the energy-scale of orbital fluctuations

is $\sim T$. The s_{++} state is consistent with the robustness of T_c against the randomness in Fe-pnictides [39–44].

Figure 4 (e) shows the gap functions for $x = 0.14$. Although the spin fluctuation is stronger because of the relation $\alpha_c \ll \alpha_s$, the obtained gap structure is very different from the so-called s_{\pm} -wave state [45–47], in which the gaps of the three hole-FSs are the same in sign. This gap structure is induced by the cooperation of the “attractive interaction between h-FS3 and e-FS” due to orbital fluctuations and “repulsive interaction between h-FS1,2 and e-FS” due to spin fluctuations [31]. This gap structure may easily change to the s_{++} -wave state by introducing small amount of impurities and e -ph interaction [42].

We also performed the similar analysis for $\text{SmFeAsO}_{1-x}\text{H}_x$, which shows the single-dome T_c , by constructing the first-principle tight-binding models. In Sm-compounds, h-FS3 is very large due to the shorter anion-height [48], and the inter- and intra-orbital nesting is improved. Since the strong orbital fluctuations appear even at $x \sim 0.2$, λ_E of $\text{SmFeAsO}_{1-x}\text{H}_x$ becomes larger as shown in the inset of Fig. 4 (c), and the single-dome T_c structure is well reproduced. This result indicates the importance of the d_{xy} -orbital FS to realize higher T_c .

In summary, we studied the phase diagram of $\text{LaFeAsO}_{1-x}\text{H}_x$ using the SC-VC $_{\Sigma}$ method, and predicted that the non-nematic $O_{3z^2-r^2}$ order triggers the new C_4 isostructural transition at $x \sim 0.5$ [17]. Also, we obtain the approximate s_{++} -wave gap structure due to orbital fluctuations for both $x \gtrsim 0$ and $x \lesssim 0.5$ by taking the Δ -VC into account. The switch of the dominant quadrupole fluctuations in Fig. 2 gives the minimum structure of T_c around $x \sim 0.2$. The non-nematic orbital fluctuations will be a key ingredient in realizing high- T_c ($\sim 50\text{K}$) in H-doped La1111 , Sm1111 , as well as Ca122 .

We are grateful to H. Hosono, J. Yamaura, Y. Murakami, N. Fujiwara, H. Hiraga and S. Iimura for useful discussions. This study has been supported by Grants-in-Aid for Scientific Research from MEXT of Japan.

-
- [1] Y. Mizuguchi and Y. Takano, J. Phys. Soc. Jpn. **79**, 102001 (2010).
 - [2] R. M. Fernandes, L. H. VanBebber, S. Bhattacharya, P. Chandra, V. Keppens, D. Mandrus, M. A. McGuire, B. C. Sales, A. S. Sefat, and J. Schmalian, Phys. Rev. Lett. **105**, 157003 (2010).
 - [3] F. Krüger, S. Kumar, J. Zaanen, J. van den Brink, Phys. Rev. B **79**, 054504 (2009).
 - [4] W. Lv, J. Wu, and P. Phillips, Phys. Rev. B **80**, 224506 (2009).
 - [5] C.-C. Lee, W.-G. Yin, and W. Ku, Phys. Rev. Lett. **103**, 267001 (2009).
 - [6] S. Onari and H. Kontani, Phys. Rev. Lett. **109**, 137001 (2012).
 - [7] S. Liang, A. Moreo, and E. Dagotto, Phys. Rev. Lett. **111**, 047004 (2013).

- [8] M. Yoshizawa, D. Kimura, T. Chiba, S. Simayi, Y. Nakanishi, K. Kihou, C.-H. Lee, A. Iyo, H. Eisaki, M. Nakajima, and S. Uchida, *J. Phys. Soc. Jpn.* **81**, 024604 (2012).
- [9] A. E. Böhmer, P. Burger, F. Hardy, T. Wolf, P. Schweiss, R. Fromknecht, M. Reinecker, W. Schranz, and C. Meingast, *Phys. Rev. Lett.* **112**, 047001 (2014).
- [10] M. Yi, D. Lu, J.-H. Chu, J. G. Analytis, A. P. Sorini, A. F. Kemper, B. Moritz, S.-K. Mo, R. G. Moore, M. Hashimoto, W.-S. Lee, Z. Hussain, T. P. Devereaux, I. R. Fisher, and Z.-X. Shen, *Proc. Natl. Acad. Sci. USA* **108**, 6878 (2011).
- [11] T. Shimojima, T. Sonobe, W. Malaeb, K. Shinada, A. Chainani, S. Shin, T. Yoshida, S. Ideta, A. Fujimori, H. Kumigashira, K. Ono, Y. Nakashima, H. Anzai, M. Arita, A. Ino, H. Namatame, M. Taniguchi, M. Nakajima, S. Uchida, Y. Tomioka, T. Ito, K. Kihou, C. H. Lee, A. Iyo, H. Eisaki, K. Ohgushi, S. Kasahara, T. Terashima, H. Ikeda, T. Shibauchi, Y. Matsuda, and K. Ishizaka, *Phys. Rev. B* **89**, 045101 (2014).
- [12] Y. Gallais, R. M. Fernandes, I. Paul, L. Chauviere, Y.-X. Yang, M.-A. Measson, M. Cazayous, A. Sacuto, D. Colson, and A. Forget, *Phys. Rev. Lett.* **111**, 267001 (2013).
- [13] H. Kontani and Y. Yamakawa, arXiv:1312.0528.
- [14] S. Kasahara, H. J. Shi, K. Hashimoto, S. Tonegawa, Y. Mizukami, T. Shibauchi, K. Sugimoto, T. Fukuda, T. Terashima, A. H. Nevidomskyy, and Y. Matsuda, *Nature* **486**, 382 (2012).
- [15] S. Iimura, S. Matuishi, H. Sato, T. Hanna, Y. Muraba, S. W. Kim, J. E. Kim, M. Takata, and H. Hosono, *Nat. Commun.* **3**, 943 (2012).
- [16] N. Fujiwara, S. Tsutsumi, S. Iimura, S. Matsuishi, H. Hosono, Y. Yamakawa, and H. Kontani, *Phys. Rev. Lett.* **111**, 097002 (2013).
- [17] M. Hiraishi, S. Iimura, K. M. Kojima, J. Yamaura, H. Hiraka, K. Ikeda, P. Miao, Y. Ishikawa, S. Torii, M. Miyazaki, I. Yamauchi, A. Koda, K. Ishii, M. Yoshida, J. Mizuki, R. Kadono, R. Kumai, T. Kamiyama, T. Otomo, Y. Murakami, S. Matsuishi and H. Hosono, *Nat. Phys.* **10**, 300 (2014).
- [18] For $x > 0.5$, in addition to the c -axis length change, Fe-layers and As-layers slide alternatively at T_S [17]. The latter may be due to band-JT effect since the lattice deformation is very large.
- [19] S. R. Saha, N. P. Butch, T. Drye, J. Magill, S. Ziemak, K. Kirshenbaum, P. Y. Zavaliy, J. W. Lynn, and J. Paglione, *Phys. Rev. B* **85**, 024525 (2012).
- [20] K. Kudo, K. Iba, M. Takasuga, Y. Kitahama, J. Matsuura, M. Danura, Y. Nogami, and M. Nohara, *Sci. Rep.* **3**, 1478 (2013).
- [21] S. Avci, O. Chmaissem, S. Rosenkranz, J. M. Allred, I. Eremin, A. V. Chubukov, D.-Y. Chung, M. G. Kanatzidis, J.-P. Castellán, J. A. Schlueter, H. Claus, D. D. Khalyavin, P. Manuel, A. Daoud-Aladine, and R. Osborn, arXiv:1303.2647
- [22] Y. Yamakawa, S. Onari, H. Kontani, N. Fujiwara, S. Iimura, and H. Hosono, *Phys. Rev. B* **88**, 041106(R) (2013).
- [23] K. Suzuki, H. Usui, K. Kuroki, S. Iimura, Y. Sato, S. Matsuishi, and H. Hosono, *J. Phys. Soc. Jpn.* **82**, 083702 (2013).
- [24] K. Suzuki, H. Usui, S. Iimura, Y. Sato, S. Matsuishi, H. Hosono, and K. Kuroki, arXiv:1311.2413.
- [25] S. Simayi, K. Sakano, H. Takezawa, M. Nakamura, Y. Nakanishi, K. Kihou, M. Nakajima, C. Lee, A. Iyo, H. Eisaki, S. Uchida, and M. Yoshizawa, *J. Phys. Soc. Jpn.* **82**, 114604 (2013).
- [26] A. O. Sboychakov, A. V. Rozhkov, K. I. Kugel, A. L. Rakhmanov, and F. Nori, *Phys. Rev. B* **88**, 195142 (2013).
- [27] H. Kontani and S. Onari, *Phys. Rev. Lett.* **104**, 157001 (2010).
- [28] Y. Ohno, M. Tsuchiizu, S. Onari, and H. Kontani, *J. Phys. Soc. Jpn.* **82**, 013707 (2013).
- [29] M. Tsuchiizu, Y. Ohno, S. Onari, and H. Kontani, *Phys. Rev. Lett.* **111**, 057003 (2013).
- [30] The nonzero matrix elements of \hat{O}_γ with respect to $2 \sim 4$ orbitals are $O_{x^2-y^2}^{2,2} = -O_{x^2-y^2}^{3,3} = 1$, $2O_{3z^2-r^2}^{2,2} = 2O_{3z^2-r^2}^{3,3} = -O_{3z^2-r^2}^{4,4} = 1$, and $O_{xz}^{3,4} = O_{xz}^{4,3} = 1$ [27].
- [31] T. Saito, S. Onari, Y. Yamakawa, H. Kontani, S.V. Borisenko, and V.B. Zabolotnyy, arXiv:1402.2398.
- [32] Supplemental Material at <http://link.aps.org/supplemental/>
- [33] H. Kontani, T. Saito, and S. Onari, *Phys. Rev. B* **84**, 024528 (2011).
- [34] C. Ma, L. Wu, W.-G. Yin, H. Yang, H. Shi, Z. Wang, J. Li, C.C. Homes, and Y. Zhu, *Phys. Rev. Lett.* **112**, 077001 (2014).
- [35] K. I. Kugel and D. I. Khomskii, *Sov. Phys. Usp.* **25**, 231 (1982).
- [36] E. Shender, *Sov. Phys. JETP* **56**, 178 (1982); C. L. Henley, *Phys. Rev. Lett.* **62**, 2056 (1989); A. Moreo, E. Dagotto, T. Jolicoeur and J. Riera, *Phys. Rev. B* **42**, 6283 (1990); P. Chandra, P. Coleman, and A.I. Larkin, *Phys. Rev. Lett.* **64**, 88 (1990).
- [37] C.-Y. Moon and H.J. Choi, *Phys. Rev. Lett.* **104**, 057003 (2010); W.-G. Yin, C.-C. Lee, and W. Ku, *Phys. Rev. Lett.* **105**, 1070004 (2010).
- [38] T. Saito, S. Onari, and H. Kontani, *Phys. Rev. B* **88**, 045115 (2013).
- [39] A. Kawabata, S. C. Lee, T. Moyoshi, Y. Kobayashi, and M. Sato, *J. Phys. Soc. Jpn.* **77**, 103704 (2008).
- [40] Y. Nakajima, T. Taen, Y. Tsuchiya, T. Tamegai, H. Kitamura, and T. Murakami, *Phys. Rev. B* **82**, 220504 (2010).
- [41] J. Li, Y.F. Guo, S.B. Zhang, J. Yuan, Y. Tsujimoto, X. Wang, C.I. Sathish, Y. Sun, S. Yu, W. Yi, K. Yamaura, E. Takayama-Muromachi, Y. Shirako, M. Akaogi, and H. Kontani, *Phys. Rev. B* **85**, 214509 (2012).
- [42] S. Onari and H. Kontani, *Phys. Rev. Lett.* **103**, 177001 (2009).
- [43] Y. Yamakawa, S. Onari, and H. Kontani, *Phys. Rev. B* **87**, 195121 (2013).
- [44] Y. Wang, A. Kreisel, P. J. Hirschfeld and V. Mishra, *Phys. Rev. B* **87**, 094504 (2013): They reported that the the conventional s_{\pm} -wave state becomes very robust against the Unitary scatters since they used oversimplified two-band model. This artifact due to the oversimplified model is explained in Sec. V.C of Ref. [43] in detail.
- [45] K. Kuroki, S. Onari, R. Arita, H. Usui, Y. Tanaka, H. Kontani, and H. Aoki, *Phys. Rev. Lett.* **101**, 087004 (2008).
- [46] P. J. Hirschfeld, M. M. Korshunov, and I. I. Mazin, *Rep. Prog. Phys.* **74**, 124508 (2011).
- [47] A. V. Chubukov, D. V. Efremov, and I. Eremin, *Phys. Rev. B* **78**, 134512 (2008).
- [48] S. Matsuishi, T. Maruyama, S. Iimura and H. Hosono, *Phys. Rev. B* **89**, 094510 (2014).

[SUPPLEMENTAL MATERIAL] NUMERICAL
STUDY OF $\text{LaFeAsO}_{1-x}\text{H}_x$: COMPARISON
BETWEEN DIFFERENT TYPES OF
FLUCTUATION THEORIES

**A: fluctuation-exchange (FLEX) approximation for
 $\text{LaFeAsO}_{1-x}\text{H}_x$**

In the main text, we studied the models of $\text{LnFeAsO}_{1-x}\text{H}_x$ ($\text{Ln}=\text{La}, \text{Sm}$) based on the SC- VC_Σ method, in which both the VC and self-energy are calculated self-consistently. Since the nematic and non-nematic orbital orders are induced by the VC, experimental C_2 - and C_4 -structure transitions are naturally explained. In addition, orbital-fluctuation-mediated s_{++} -wave state is obtained.

The FLEX approximation had been used in the study of Fe-based superconductors [24]. Considering that the FLEX approximation cannot explain the C_2 and C_4 -structure transition due to the neglect of the VC, it would be incomplete for the study of the superconductivity realized near the structural QCPs. With knowledge of this defect, we solve the linearized gap equation within the FLEX approximation.

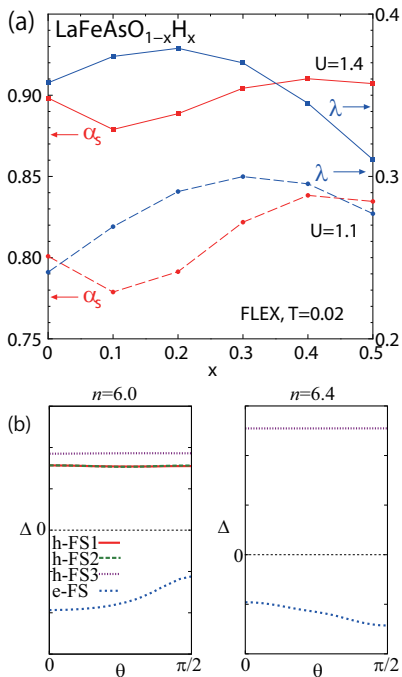


FIG. 5: (color online) (a) x -dependences of the spin Stoner factor α_S and the eigenvalue λ_E given by the FLEX approximation. (b)(c) Gap functions given by the FLEX approximation for $x = 0$ and 0.4 in the case of $U = 1.4$.

We use 64×64 \mathbf{k} -meshes and 512 Matsubara frequencies, and fix $T = 0.02\text{eV}$ to avoid artifacts due to the shortage of the \mathbf{k} -mesh number. We fix the ratio $J/U = 1/6$. Figure 5 (a) shows the obtained spin Stoner factor α_S and the eigenvalue of the gap equation λ_E for

$n = 6.0 \sim 6.5$ ($x = 0 \sim 0.5$), in the case of $U = 1.1$ and 1.4 . Similar result is obtained for $T = 0.005$ and $U = 1.3$ using 32×32 \mathbf{k} -meshes, which were used by Suzuki *et al.* [24]. The obtained s_{\pm} -wave gap functions are shown in Fig. 5 (b) and (c).

The single-dome structure of λ_E in Fig. 5 (a) is different from the numerical result at $\Delta\alpha = 0$ in Ref. [24], but similar to that of $\Delta\alpha < -1^\circ$. This difference should originate from differences in the models: Suzuki *et al.* used the VASP package using a fixed Fe-As length, whereas the present authors used the WIEN2k package.

**B: self-consistent vertex-correction (SC-VC)
method for $\text{LaFeAsO}_{1-x}\text{H}_x$**

In the main text, we analyzed $\text{LaFeAsO}_{1-x}\text{H}_x$ using the SC- VC_Σ method, in which the self-energy correction is incorporated into the SC-VC method. The obtained strong ferro-quadrupole susceptibilities $\chi_{x^2-y^2}^Q(\mathbf{0})$ and $\chi_{3z^2-r^2}^Q(\mathbf{0})$ in Fig. 2 explain the C_2 and C_4 structure transitions at $x \sim 0$ and $x \sim 0.5$, respectively.

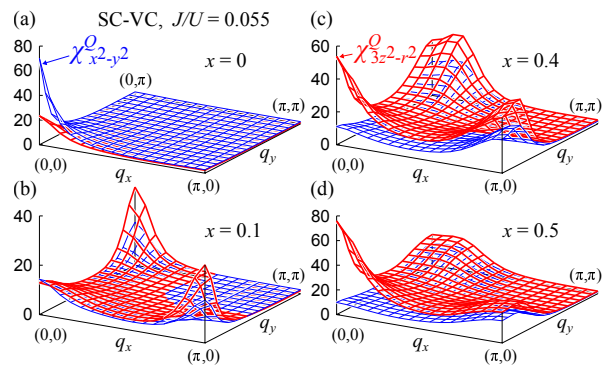


FIG. 6: (color online) for (a) $x = 0$ ($U = 1.39$), (b) $x = 0.1$ ($U = 1.34$), (c) $x = 0.4$ ($U = 1.06$) and (d) $x = 0.5$ ($U = 0.99$), obtained by the SC-VC method for $J/U = 0.055$. Stoner factors are $\alpha_c = 0.97$ and $\alpha_s \sim 0.9$. In the SC-VC method, $\chi_{xz/yz}^Q(q)$ is smaller and not shown.

Here, we show that the essentially similar quadrupole fluctuations are obtained by using the SC-VC method, in which the self-energy is dropped [6]. Due to the self-energy, the value of U for a fixed $\max\{\alpha_c, \alpha_s\}$ in the SC- VC_Σ method is larger than that in the SC-VC method. Since the AL-term grows in proportion to U^4 , the relation $\alpha_c > \alpha_s$ is realized against larger J/U in the SC- VC_Σ method.

Figure 6 (a)-(d) shows the obtained $\chi_{3z^2-r^2}^Q(q)$ and $\chi_{x^2-y^2}^Q(q)$ for $J/U = 0.055$: The results are essentially unchanged for $0 < J/U < 0.06$. For each x , we choose U so that the charge Stoner factor satisfy $\alpha_c = 0.97$. At $x = 0$ in (a) and $x = 0.1$ in (b), we obtain large peak of $\chi_{x^2-y^2}^Q(\mathbf{0})$, and its divergence corresponds to the C_2

structure transition. At $x = 0.4$ in (c) and $x = 0.5$ in (d), we obtain the divergent peak of $\chi_{3z^2-r^2}^Q(\mathbf{0})$, which corresponds to the C_4 isostructural transition. Thus, both C_2 and C_4 structure transitions in $\text{LaFeAsO}_{1-x}\text{H}_x$ at $x \sim 0$ and $x \sim 0.5$ respectively are explained by the SC-VC method, meaning that the self-energy correction is not essential for them.

In addition, strong antiferro-quadrupole susceptibilities $\chi_{3z^2-y^2}^Q(\mathbf{Q})$ and $\chi_{x^2-y^2}^Q(\mathbf{Q})$ appears for $x \geq 0.1$ in Fig. 6 (b)-(d). On the other hand, $\chi_{xz/yz}^Q(\mathbf{Q})$ remains small, although it is strongly enhanced in the SC-VC $_{\Sigma}$ method shown in Fig. 2 (a). It is considered that this discrepancy originates from the neglect of the self-energy in the SC-VC method: In the SC-VC $_{\Sigma}$ method, the strong d_{xy} -orbital spin susceptibility $\chi_{4,4,4,4}^s$ in the RPA are suppressed by the d_{xy} -orbital self-energy. Due to this negative feedback effect, $\chi_{4,4,4,4}^s$ is comparable to $\chi_{2,2,2,2}^s$ and $\chi_{3,3,3,3}^s$ in the SC-VC $_{\Sigma}$ method, and then $\Phi_{2(3)}^c \sim \Phi_4^c$. For this reason, $\chi_{xz/yz}^Q(\mathbf{Q})$ is enlarged by large $\Phi_{2(3)}^c$.

In the previous SC-VC study for $x = 0.1$ [6], we have interested in the developments of $\chi_{x^2-y^2}^Q(q)$ and $\chi_{xz,yz}^Q(q)$, so we have dropped $X_{l,l,4,4}^c(q)$ and $X_{4,4,l,l}^c(q)$. In the present study, we include $X_{l,l,4,4}^c(q)$, and find that $\chi_{3z^2-r^2}^Q(q)$ is also strongly enhanced due to large $X_{4,4,4,4}^c(q)$. However, large $\chi_{3z^2-r^2}^Q$ for $x = 0 \sim 0.1$ in Fig. 6 (b) is found to be over-estimated due to the absence of the self-energy, as confirmed by the numerical result of the SC-VC $_{\Sigma}$ method in Fig. 2 (a). Except for that, the obtained results given by the SC-VC method are similar to those by the SC-VC $_{\Sigma}$ method, and therefore they are reliable.

C: SC-VC $_{\Sigma}$ method for $J/U = 0.12$

In Fig. 2 (a) and (b) of the main text, we show the quadrupole susceptibilities given by the SC-VC $_{\Sigma}$ method in the case of $J/U = 0.14$. Here, we perform the same calculation for $J/U = 0.12$, and show the obtained results in Fig. 7. As for the ferro-quadrupole fluctuations, strong development of $\chi_{x^2-y^2}^Q(\mathbf{0})$ at $x = 0$ and that of $\chi_{3z^2-y^2}^Q(\mathbf{0})$ at $x = 0.4$ are obtained in Fig. 7, consistently with the results of $J/U = 0.14$. Also, large antiferro-quadrupole susceptibility $\chi_{xz,yz}^Q(\mathbf{Q})$ at $x = 0$ is obtained in both $J/U = 0.12$ and 0.14 , whereas $\chi_{3z^2-r^2}^Q(\mathbf{Q})$ at $x = 0.4$ is relatively small for $J/U = 0.14$. As shown in Fig. 4 (c), the x -dependence of the eigenvalue λ_E for

$J/U = 0.12$ is similar to that for $J/U = 0.14$. Thus, qualitative results of the SC-VC $_{\Sigma}$ method are unchanged for $J/U = 0.12 \sim 0.14$.

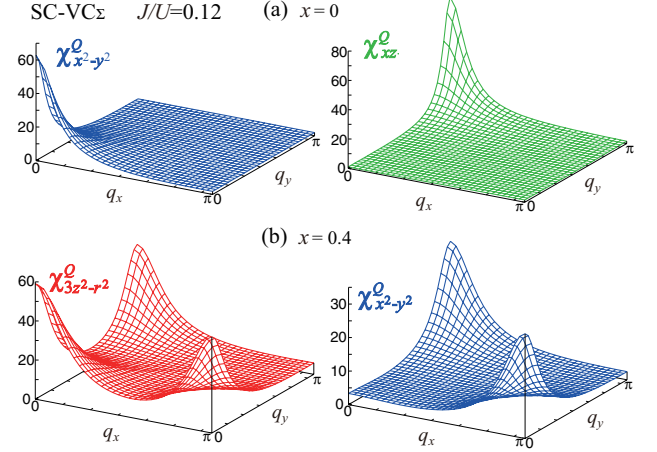


FIG. 7: (color online) $\chi_{\gamma}^Q(\mathbf{q})$ given by the SC-VC $_{\Sigma}$ method for $J/U = 0.12$: (a) $\gamma = x^2 - y^2$ and $\gamma = xz$ for $x = 0$ ($U = 2.05$), and (b) $\gamma = 3z^2 - r^2$ and $\gamma = x^2 - y^2$ for $x = 0.4$ ($U = 1.62$). In both cases, $\alpha_c = 0.97$.

D: Expressions of $\chi_{x^2-y^2}^Q(\mathbf{0})$ and $\chi_{3z^2-r^2}^Q(\mathbf{0})$ for $J > 0$

In the main text, we present the analytic expression of $\chi_{x^2-y^2}^Q(\mathbf{0})$ and $\chi_{3z^2-r^2}^Q(\mathbf{0})$ in Eqs. (3) and (4), respectively, in the case of $J = 0$ for simplicity. Here, we present their expressions for finite J :

$$\chi_{x^2-y^2}^Q(\mathbf{0}) = 2\Phi_2^c(1 - (U - 5J)\Phi_2^c)^{-1}, \quad (7)$$

$$\chi_{3z^2-r^2}^Q(\mathbf{0}) = b'(1 - a'U\Phi_4^c)^{-1}, \quad (8)$$

where $a' = \frac{1}{2} \frac{5(U - 5J)(U - 2J)\Phi_2^c - U}{(3U - 5J)\Phi_2^c + 1}$ and $b' = \frac{1}{2} \frac{2\Phi_4^c + \Phi_2^c + 15(U - 2J)\Phi_2^c\Phi_4^c}{(3U - 5J)\Phi_2^c + 1}$.

Equation (7) had been already given in Ref. [28]. Thus, $\chi_{x^2-y^2}^Q(\mathbf{0})$ diverges when $\Phi_2^c = (U - 5J)^{-1}$, and $U - 5J$ is positive when the relation $J/U = 0.12 \sim 0.15$ predicted by the first principle study by Miyake *et al* (J. Phys. Soc. Jpn. **79**, 044705 (2010)) is correct. According to the expression of a' , we find that a' is positive for $\Phi_2^c > [5(1 - 5J/U)(U - 2J)]^{-1}$ in the case of $J/U < 1/5$. Then, $\chi_{3z^2-r^2}^Q(\mathbf{0})$ diverges when $\Phi_4^c = (a'U)^{-1}$. Therefore, the discussions in the main text below Eqs. (3) and (4) is valid even for finite J .